Chinese Chemical Letters 35 (2024) 109324

Contents lists available at ScienceDirect

Chinese Chemical Letters

journal homepage: www.elsevier.com/locate/cclet

Mapping multiple phases in curcumin binary solid dispersions by fluorescence contrasting

Ying Xu[a,1], Chengying Shen[c,d,1], Hailong Yuan[c], Wei Wu[a,b,*]

[a] Key Laboratory of Smart Drug Delivery of MOE, School of Pharmacy, Fudan University, Shanghai 201203, China
[b] Center for Medical Research and Innovation, Shanghai Pudong Hospital, Fudan University Pudong Medical Center, Shanghai 201399, China
[c] Department of Pharmacy, Air Force Medical Center, PLA, Beijing 100142, China
[d] Jiangxi Provincial People's Hospital, The First Affiliated Hospital of Nanchang Medical College, Nanchang 330006, China

ARTICLE INFO

Article history:
Received 8 October 2023
Revised 10 November 2023
Accepted 15 November 2023
Available online 19 November 2023

Keywords:
Solid dispersion
Curcumin
PEG
PVP
Poloxamer
Fluorescence
Environment-responsive
Confocal laser scanning microscopy

ABSTRACT

The microphases and miscibility in binary curcumin (Cur) solid dispersions (SDs) with amorphous polyvinylpyrrolidone K30 (PVP K30) and semi-crystalline poloxamer (P407) and poly(ethylene glycol) 6000 (PEG6000) as carriers were investigated by fluorescence contrasting utilizing confocal laser scanning microscopy. A super sensitive fluorophore P4 with typical aggregation-caused quenching properties was employed to stain the continuous polymer phases and contrasted with the autofluorescence of the model drug Cur. In addition, differential scanning calorimetry (DSC) and powder X-ray diffraction (PXRD) were utilized to assist in explanation of the fluorescence results. In all three SD systems, there is always a homogenous polymer phase stained by P4 and it is difficult to adulterate Cur crystals by P4. Cur-enriched rather than polymer-enriched domains could be detected. In the Cur-PVP K30 system, Cur exists in an amorphous form at a Cur loading level of 50% and below, while Cur crystallines phase out and continuously grow with the increase of Cur loading from 60% to 90%. The phase behaviors in the Cur-P407 and Cur-PEG 6000 systems are similar but with minor differences. In both systems, Cur phases out as clusters of drug-enriched domains at a loading level of 20% and below, which however cannot be correlated with crystallization, as evidenced by both DSC and PXRD. There is a transition from an amorphous to a crystalline state from 20% to 30% Cur loading, above which Cur crystallines can be detected. It is interesting that a co-mix phase of both Cur- and PEG 6000-enriched domains can be identified at Cur loading levels of 10% and less. Taking together, it is concluded that contrasting Cur autofluorescence with the signals of P4 proves to be a functional strategy to reveal multiple phases in the binary SD systems investigated.

Solid dispersions (SDs) are commonly defined as a system with one or more solutes solubilized or dispersed in the solid continuous phases of one or more carriers, preferably highly hydrophilic or readily soluble polymers [1–5]. The general goal of SD is to achieve a highly dispersed metastable state of the solutes, which renders them readily dissolvable upon contact with aqueous media. First conceptualized by Sekiguchi and Obi in 1961 [6], SD has evolved for more than sixty years. In addition to numerous publications, a few tens of SD products have been successfully marketed as well [2–4,7,8]. Depending on the properties and mass ratio of the drugs and carriers, drugs can exist as microcrystalline, solid solution, or amorphous phases in SD [3,9]. Readers are referred to recent reviews for the state of the art [3,4,10–12]. The current challenges rest with mass production, physical instability, and restricted drug loading [13–17].

The physical state is a determining factor in SD's stability and dissolution. It is generally acknowledged that only a limited amount, usually too low to meet practical needs, of drugs can be solubilized completely in the carrier matrix to form a solid solution [18–21]. At higher loading levels, drugs commonly exist in a solidified state of high dispersibility, which however is not stable enough and prone to phasing out or recrystallization, depending on the drug/polymer ratios. In recent years, the physical state and multiple interactions within the SD systems have been identified or probed by a variety of approaches, *e.g.*, differential scanning calorimetry (DSC), powder X-ray diffraction (PXRD), Fourier transformed infrared spectroscopy (FTIR), thermogravimetric analysis (TGA), Raman spectroscopy, and fluorescence microscopy [16,22]. A concept of miscibility was devised to roughly describe the

* Corresponding author.
E-mail address: wuwei@shmu.edu.cn (W. Wu).
[1] These authors contributed equally to this work.

https://doi.org/10.1016/j.cclet.2023.109324
1001-8417/

physical states of the solutes in SD matrices [23–26]. Miscibility could be interpreted as the ability of co-mix SD systems with "excessive" (*i.e.*, above the saturation solubility) solutes to maintain a high-energy state for extended times. When too many solutes are presented (*i.e.*, above the miscibility limit), the drugs overrun the miscible capacity and phase out very quickly. Taylor's group went further to probe the heterogeneity of binary SD systems using environment-responsive fluorophores or autofluorescent model drugs [27–30]. Drug-enriched domains were visualized within the polymer matrices based on the assumption that hydrophobic fluorophores tend to accumulate in hydrophobic drug-rich domains [28]. Evidence by confocal laser scanning microscopy (CLSM) also concludes that drugs may phase out as nanoparticles [30]. On the other hand, by probing the autofluorescence of a model drug indomethacin, the physical state (*e.g.*, heterogeneity/homogeneity) of the drug in binary hydroxypropyl methylcellulose (HPMC) SD systems was revealed by correlating to the drug/polymer ratio [29].

Though environment-responsive fluorophores provide pertinent information that helps clarify the virtual physical phases within the SD matrix, the adulteration of fluorophores has its limitations. One concern is the lack of sufficient environmental responsiveness to discriminate multiple drug- or polymer-associated phases. Other concerns include the undue loading (0.2%–0.5%) [28–32] of the fluorophores owing to their low quantum yields, which may influence the phase behaviors. Moreover, the information reported by current fluorescence methods is limited owing to the use of mono-channel signals of either the fluorophore or the drug. Therefore, we hypothesize that multiple phases in SDs may be revealed in more detail by labeling the carrier matrix with more sensitive and brighter fluorophores and contrasting them with drug-associated phases, taking advantage of the disparity in fluorescence responsiveness between different phases and autofluorescence of the drugs.

Herein, we investigate the virtual physical states in binary curcumin (Cur, Fig. 1) SDs. Cur was chosen as the model drug because of not only its autofluorescence but also the easy formation of intramolecular hydrogen bonds and therefore easy phasing out to display multiple phases [33]. A very bright environment-responsive fluorophore, P4 (Fig. 1), with a dipyrromethene boron difluoride (BODIPY) parent structure [34,35] was employed to stain and visualize the multiple phases in the SDs. In addition to high quantum yield, near-infrared emission, and photostability, the most distinguishable feature of this fluorophore is its high environment-responsiveness. Owing to its high hydrophobicity, it stays in a solubilized and emissive state in hydrophobic media but forms aggregates immediately upon contact with water, which directly results in aggregation-caused quenching (ACQ) with fluorescence decreasing to near zero [36–38]. This phenomenon implies that this kind of fluorophore is exceptionally sensitive to the changes in environmental polarity and may function to probe the multiple phases in SDs. ACQ-based fluorophores have been employed to label and track drug nanocarriers in bioimaging studies by several groups [39–46]. A loading level of 0.001%–0.002% is enough to accommodate *in vivo* bioimaging. It is envisioned that by contrasting or co-localizing Cur autofluorescence with P4 fluorescence, the physical state of the drug crystals, co-crystals, and/or co-amorphous phases as well as the solubilized state can be revealed in more detail. In the current study, three common SD systems with polyethylene glycol (PEG) 6000, polyvinylpyrrolidone (PVP) K30, and polyoxyethylene polyoxypropylene copolymer (Poloxamer) 407 (Fig. 1) as carriers are investigated.

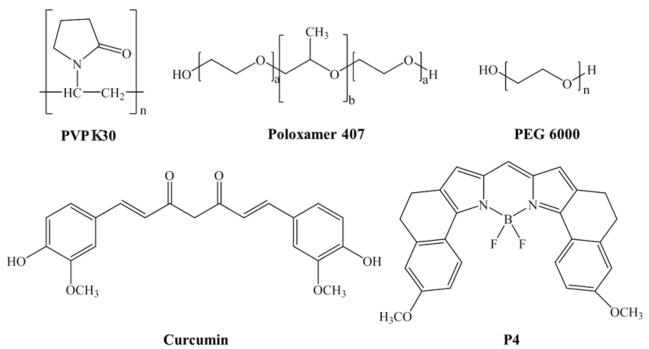

Fig. 1. Chemical structures of PVP K30, P407, PEG6000, curcumin, and the environment-responsive fluorophore P4.

The environment-responsiveness of the fluorophore P4, as well as Cur, was studied by monitoring their sensitivity to water. The emission spectra of both Cur and P4 in aqueous acetonitrile with different water fractions are acquired and displayed in Figs. 2A and B, respectively. The maximum emission wavelength (λ_{em}) of Cur is about 525 nm at an excitation wavelength of 405 nm (Fig. 2A). In response to the increase of water fraction from 0 to 100%, the fluorescence intensity of Cur decreases gradually with λ_{em} increasing from about 520 nm to 530 nm. The autofluorescence of Cur bears a certain degree of environmental responsiveness too, but there is no water fraction-related jump in both fluorescence intensity and wavelength (Fig. 2C). The λ_{em} of P4 is 660 nm at an excitation wavelength of 603 nm (Fig. 2B). The fluorescence intensity of P4 remains at a level of more than 80% of its original at a water fraction of 70% and below but drops abruptly at a water fraction of 80%. At a water fraction of 90% and above, the fluorescence intensity of P4 drops to near zero, demonstrating superior water sensitivity, which on the other hand reflects P4's sensitivity to different degrees of hydrophobicity/hydrophilicity.

To facilitate CLSM observation, SDs were prepared directly on glass slides as thin films. The Cur-PVP K30 SD films were prepared by a solvent co-precipitation method, while Cur-PEG6000 or Cur-P407 SD films were prepared by a solvent melting/congealing method. SD powders for DSC and PXRD analysis were prepared under similar conditions by rotary evaporation, followed by manual milling. Please refer to Supporting information for preparation and characterization details.

Fig. 3 presents the CLSM images of the film casts of pure Cur, Cur + P4, PVP K30 + P4, P407 + P4, and PEG6000 + P4 in either 405 nm (Cur) or 633 nm (P4) channels, colorized blue or red, respectively. Pure Cur displays its fluorescence (blue) but no emission in the P4 channel (red), whereas P4-carrier systems display

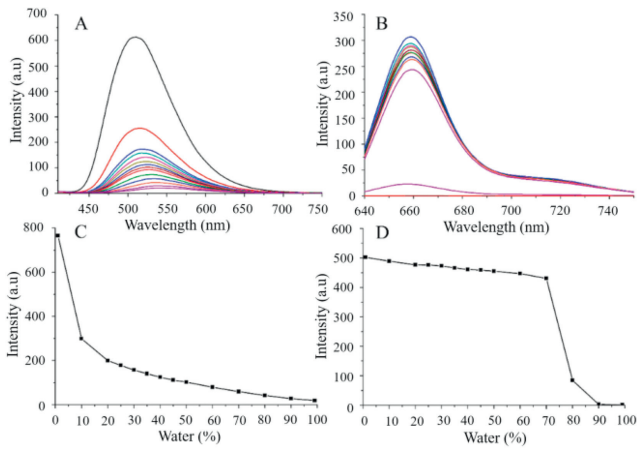

Fig. 2. The emission spectra of Cur (A) and P4 (B) at an excitation wavelength of 405 nm and 633 nm, respectively, in aqueous acetonitrile as a function of water volume fraction. The plots of fluorescence intensity of Cur (C) and P4 (D) at maximum emission wavelength *vs.* water fraction.

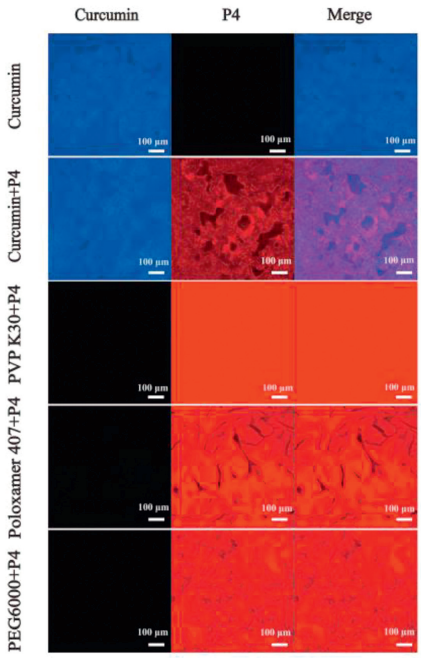

Fig. 3. Confocal laser scanning micrographs of the film casts of pure Cur, Cur + P4, PVP K30 + P4, P407 + P4, and PEG6000 + P4 in both 405 nm and 633 nm channels. Scale bar: 100 μm.

P4's emission but no Cur signals. It is implied that the signals of Cur and P4 can be collected in separate channels without mutual interference, which is verified by the emission of Cur + P4 films that demonstrates distinct signals in each channel. The pure Cur cast displays full-screen Cur signals, but the difference in fluorescence density reveals the physical details within the cast. It is obvious that Cur crystals could be seen from the CLSM images of the Cur cast. The Cur + P4 cast indicates a physical state similar to pure Cur from the Cur channel. P4 could adulterate a fraction of Cur as observed by the co-localization of signals from both channels (purple), but P4 fails to stain bulk Cur crystals because the co-localization image shows non-stained Cur domains. The full-screen red color confirms the homogenous distribution of P4 in the PVP K30 film cast, which serves as an indicator of absolute solubilization of the dye in the PVP K30 matrix. The dark fingerprints in the images of P407 + P4 and PEG 6000 + P4 at 633 nm and merged channels indicate the heterogeneous nature of both poloxamer- and PEG-based SDs owing to the semi-crystallinity of these two polymers [32]. The black stripes may represent void spaces on the plane of laser scanning left by melting/congealing, corresponding to the crevices as well as sags and crests which are observable by the naked eye.

The CLSM images of Cur-PVP K30 binary SD systems are shown in Fig. 4A. The fluorescence of films with a 5%–50% drug loading is homogeneous with blue, red, and purple colors for Cur, P4, and merged channels, respectively, indicating that Cur is uniformly dissolved or dispersed in these films. This finding is verified by results obtained from DSC and PXRD measurements (Figs. 4B and C). The DSC curves and PXRD patterns of PVP K30 did not show the endothermic peaks characteristic of melting and diffraction peaks, respectively, indicative of its amorphous structure. It is implied that at 5%–50% loading levels, Cur exists in an amorphous form in the Cur-PVP K30 binary system. However, the fluorescence becomes heterogeneous for samples with a drug loading of 60% or higher, whereby samples display either blue (Cur), red (P4), or dark domains. The dark images with faint red fluorescence are attributed to the reduced total amount of P4 utilized. As the dye P4 is believed to dissolve mainly in the polymers at a limited level and could not be easily incorporated into the crystal lattices of small molecules [40,47,48], we fixed the loading level of P4 in the polymers. Unfortunately, the low PVP K30 level determines the low level of P4 too, which makes the fluorescence from the P4 channel too low to be detected by CLSM. At a 60% drug loading level, the appearance of dark points in the visual field may suggest the beginning of phase separation in the binary system. This tendency is approved by observations in both 70% and 80% loading levels which demonstrate separated Cur domains. The Cur aggregates presented in irregular shapes against the dark background are proved by DSC and PXRD to bear a certain degree of crystallinity (Figs. 4B and C). The DSC curve of crystalline Cur shows an endothermic peak at 170.07 °C, ascribable to its melting point [49,50]. At Cur loading levels of 60%, 70%, 80%, and 90%, peaks appear at 174.21, 171.25, 170.54, and 169.47 °C, respectively, corresponding to endotherms of Cur crystals in the binary system. The PXRD pattern of crystalline Cur (100%) exhibits multiple distinct peaks at 2θ scattered angles of 8.9°, 12.3°, 14.6°, 17.3°, 18.2°, 19.6°, 24.5°, 25.6°, and 26.8° [51]. Films with drug loadings ranging from 60% to 90% show the typical diffraction peaks of crystalline Cur in ascending intensities. Taking together, there is a transition from amorphous to crystalline between a Cur loading level of 50%–60%.

The CLSM images of Cur-P407 binary SD systems are shown in Fig. 5A. In the Cur channel, the heterogeneous distribution of Cur-enriched domains at 5%–20% Cur loading levels against the homogenous background, which is stained red by P4 and represents the continuous phase of P407, demonstrates the occurrence of phase separation. With the help of DSC and PXRD, the physical state of Cur within the P407 matrix could be identified. P407 is semi-crystalline in nature [52] and shows an endothermal peak ascribed to its melting point at around 52 °C. The SDs with 5%, 10%, 20%, and 30% Cur loading have endotherms at a temperature below the melting point of pure P407 but no endotherms at the corresponding position of Cur's melting point of 174.21 °C (Fig. 5B). The endothermal characteristics suggest a lack of crystallinity at low Cur loading levels (≤30%). As DSC may overlook the endothermal fingerprints of microcrystalline in SDs, PXRD results are employed to identify the physical state of Cur further (Fig. 5C). It is apparent that at a Cur level of 20% and below no diffraction is recorded, confirming the lack of crystallinity as observed by DSC. Disparity rests with the observation at 30% loading, where weak diffraction of Cur crystallines could be detected. Referring to the CLSM observations, a loading level of around 20% seems to be a dividing point regarding phase separation in the Cur-P407 binary systems. A transition is expected between the loading range of 20% and 30%.

At a loading level of 30%, Cur exists as small crystallines with sizes of about 10 μm. There is a growing tendency in crystal size when Cur loading keeps increasing. At a 40% loading level, clusters of Cur crystal needles could be observed with a diameter of tens of microns and a length of hundreds of microns. Needle-, rod- or slab-like Cur crystals could be observed in the Cur channel for 40%–90% drug-loading films. Combining the results from DSC and PXRD (Figs. 5B and C), Cur remains mainly as crystals in higher loading (≥30%) binary systems. The crystal morphology cannot be displayed in the Cur channel because multiple phases of Cur are all shown in blue. The dark shadows in the P4 channel represent images of the Cur crystals which however could be more clearly identified from the merged channel. As the drug loading increases from 40% to 70%, the rod-shaped crystals grew. When the drug loading increased to 90%, Cur formed large and irregular plate-like crystals.

The multiple phases revealed by CLSM for Cur-PEG600 binary systems are similar to those of Cur-P407, but minor differences are identified. Cur-enriched clusters are observed at a Cur loading level of 20% and below (Fig. 6A), which is similar to the behaviors of Cur-P407 (Fig. 5A). Nevertheless, the merged channel in-

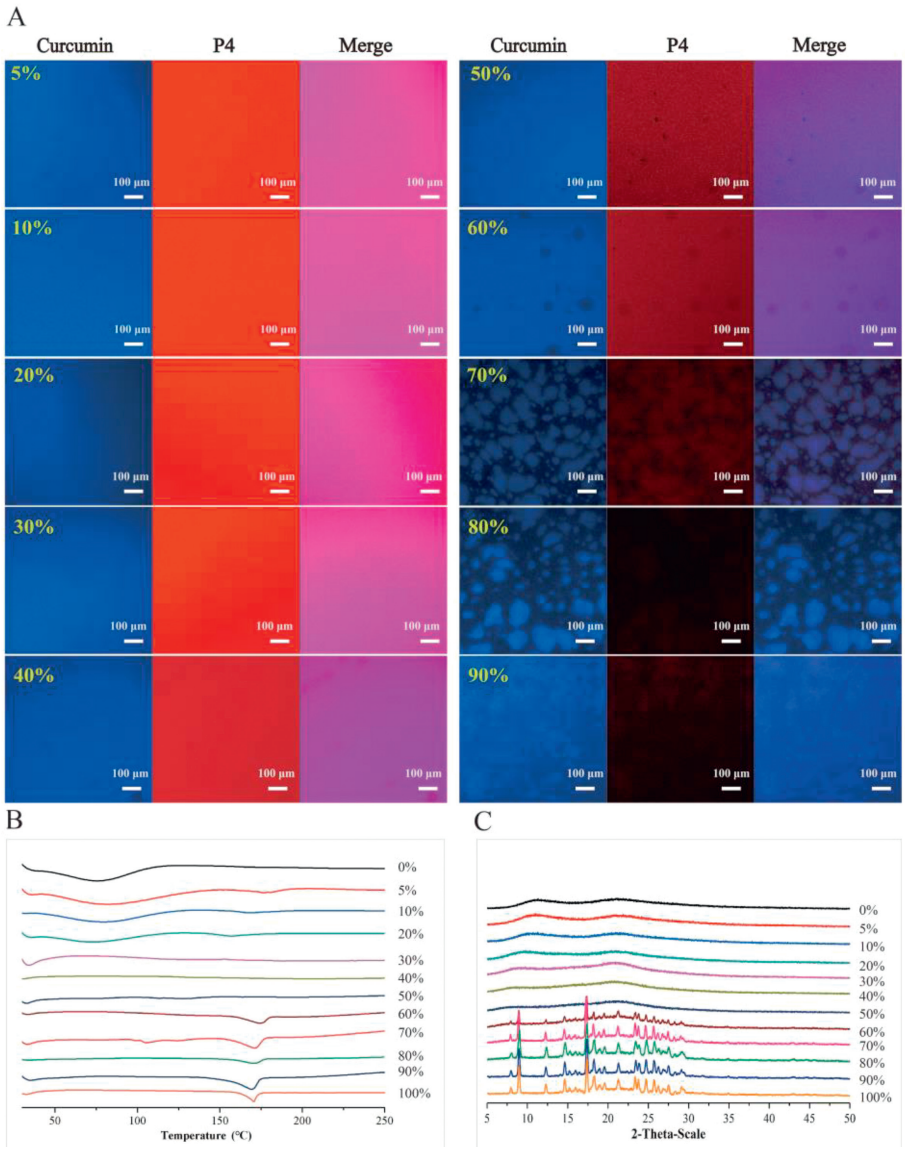

Fig. 4. (A) Confocal laser scanning micrographs of Cur-PVP K30 films at different drug loading. (B) DSC curves and (C) PXRD patterns of Cur-PVP K30 SDs. Percentages refer to drug loading. Scale bar: 100 μm.

dicates that except for the Cur-enriched clusters, purple staining of co-localization of Cur and P4 indicates the separation of the Cur-PEG6000 mixture as a new phase at a Cur level of 10%. The Cur/PEG6000 co-mix phase presents as small purple dots in the CLSM images with diameters of 10–20 μm. Both the DSC and PXRD curves do not display characteristic peaks of Cur crystallines, similar to observations with Cur-P407 (Figs. 6B and C). Cur presents as aggregates in the binary system at a loading level of 30% and above, and the size of aggregates increases with the increase of Cur loading, as revealed by the dark inlays in the P4 channel and better revealed in the merged channel. Endotherms detected by DSC emerge at a Cur loading level of 50%, in contrast with 40% for the Cur-P407 system. PXRD gives diffraction of Cur crystals at a loading level of 30%, similar to the Cur-P407 system.

Phase behaviors of drug-polymer blends play an important role in the physical stability of SDs. Intimate mixing of drug and polymer at the molecular level is deemed to be critical for optimal performance, especially the inhibition of drug crystallization during storage and dissolution [32]. When the phase separation takes place in SD, the crystallization inhibition effect of the polymer on the drug is weakened. Since most drugs are hydrophobic, phase separation into drug-rich and polymer-rich phases would result in a lower drug dissolution rate due to decreased wettability. Nevertheless, the detection of phase separation remains a challenge for the lack of functional analytical tools. Though PXRD and DSC are sensitive in reporting crystallinity and melting behaviors of SD systems, it is difficult to detect phase behaviors at microscopic levels.

The fluorescence method has been proved helpful in probing various microphases in the SD systems, such as the well-acknowledged drug-rich phases, by exploiting the environment-responsiveness of fluorophores such as pyrene and Nile red. The fluorophores are usually embedded into the carrier matrix of SDs. Alternatively, the autofluorescence of drugs could be employed to display their virtual physical states too. Despite previous endeavors, the information revealed by fluorescence probes is not always as reliable as desired owing to not only the complex mechanisms underlying environment responsiveness but also the unilateral behaviors of either carrier-associated fluorophores or drug autofluorescence. The current study greatly promotes environment-responsiveness by utilizing a more sensitive and brighter probe

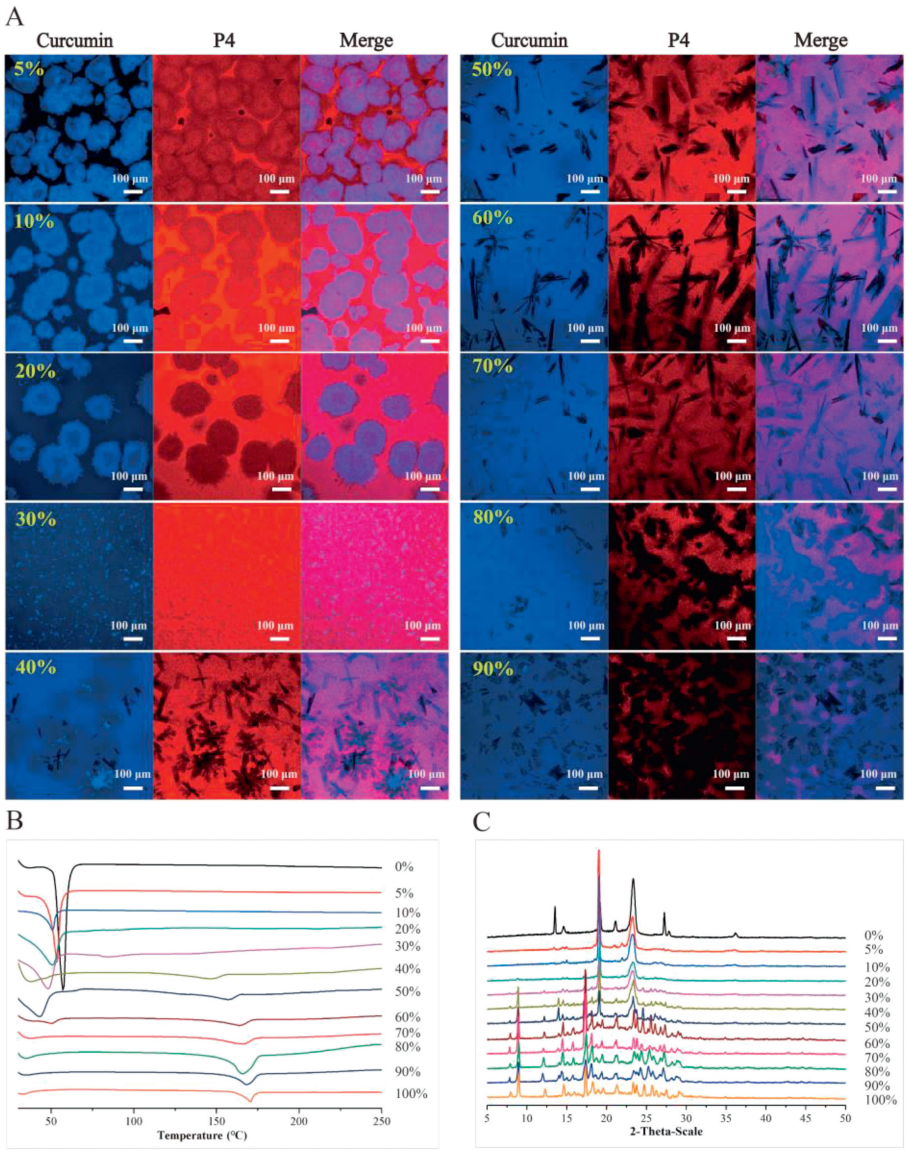

Fig. 5. (A) Confocal laser scanning micrographs of Cur-P407 films at different drug loading. (B) DSC curves and (C) PXRD patterns of Cur-P407 SDs. Percentages refer to drug loading. Scale bar: 100 μm.

P4. Compared with pyrene [37] and Nile red [53], P4 [34] possesses high water sensitivity, which reflects its higher responsiveness to environmental hydrophilicity/hydrophobicity. Though P4 is just an alternative probe in the current study that only deals with the physical state of SD, it would be very useful in downstream studies that involve an aqueous environment such as *in vitro* dissolution test. In previous studies, the conclusion of enrichment of fluorophores in "drug-rich" domains is imaginative. Nevertheless, the exploitation of drug-derived autofluorescence helps highlight the drug-associated phases by fluorescence co-localization and increasing contrast ratios.

In previous studies, CLSM was utilized to investigate the phase morphology and behavior of each component under different conditions by selectively staining drug-rich and polymer-rich phases with dyes aiming to visualize the different components [30,31,54,55]. As claimed in these studies, hydrophobic probes such as Nile red preferentially associate with the drug-rich phases leading to discrete domains, while the hydrophilic probes such as Alexa Fluor 488 bind to polymer-rich phase and form continuous domains. However, it would be considerably demanding to enrich the probes in drug-rich domains in the solid SD network because of the physical hindrance and a lack of adequate driving force in an aqueous environment. Moreover, there are unclarities regarding the degree of staining of different phases within the SD matrix, such as the pure drug phase, the drug-enriched polymer phase, and the hydrophobic phases formed by some kind of polymers themselves. In this study, auto-fluorescent Cur was used as a model drug, which shows fluorescence resulting from excitation at 405 nm in CLSM. Besides, fluorescent probe P4 was added to the SD system with the emission of red fluorescence under excitation at 633 nm. The amount of P4 is merely 1% to 10% of that reported in the literature [30–32,54,55], and the effect on phase separation is even smaller.

As literature loading of fluorophores (pyrene, Prodan, Nile red, *etc.*) is much lower than the common solubility of chemical entities in binary SD (0.2%–0.5%) [28–32], it is assumed that the probes can be solubilized in the matrix in a much stable state. Although the probes are prone to association with drug-rich phases, uncertainties arise regarding the degree of staining of different phases within the SD matrix, such as the pure drug phase, drug-enriched polymer phase, hydrophobic phases formed by polymers

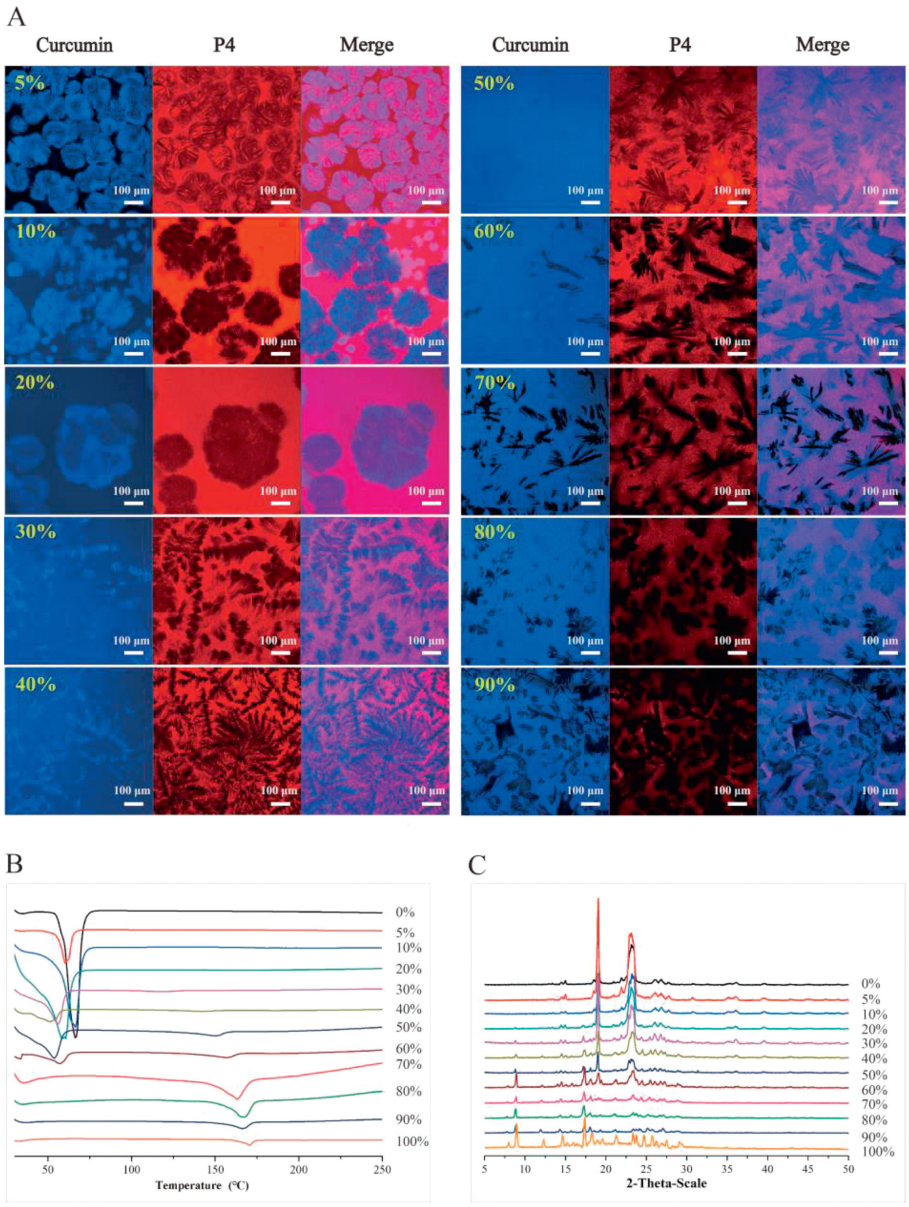

Fig. 6. (A) Confocal laser scanning micrographs of Cur-PEG6000 films at different drug loading. (B) DSC curves and (C) PXRD patterns of Cur-PEG6000 SDs. Percentages refer to drug loading. Scale bar: 100 μm.

themselves, and continuous polymer phases. Despite that fluorophores work well to identify drug-rich domains in liquid supersaturation systems [56–59], it might not be easy to enrich the probes in drug-rich domains in the solid SD network because of the physical hindrance.

There are three basic categories of phases in the binary systems investigated in this study: (1) the continuous carrier phases stained by P4; (2) the drug-associated phases; (3) the mixed drug/polymer phases as revealed by co-localization of the fluorescence of P4 and Cur. As the loading level of P4 in all three polymers is very low, the dye could be solubilized and distributed uniformly in the carrier matrix, as revealed by the fluorescence image of P4-stained carriers (Fig. 3). If there is no solute in the carrier matrix, there is no forced phasing out either. Therefore, we keep a constant loading level of P4 in the polymers.

PVP K30 is the most common precipitating inhibitor being used to prevent drug crystallization *via* its inherent hydrophilic nature by arresting reorientation and forming stronger drug-polymer interactions [60]. For the Cur-PVP K30 films, phase separation was not observed for samples with a drug loading between 5% and 50%, and polymer (PVP K30) exhibited a good stabilizing effect to retain Cur under the amorphous polymorph within the solid dispersion. However, P407 and PEG6000 gave poor stabilizing effects on Cur, and phase separation occurred at low drug loadings. After phase separation of the system, a blue drug-rich phase appeared in the Cur channel, while the corresponding region in the P4 channel did not appear bright red, and the color was darker than the surrounding continuous phase, which indicated that the hydrophobic fluorescent probe P4 was not enriched in drug-rich regions. The probe may be dispersed into the polymer in a relatively stable state and indicative of the polymer phase. Further study and evaluation would render more insight into detailed probe distribution and the microphase evolution of SDs under long-aging, high-temperature, and high-humidity conditions.

The preparative procedures influence the phase behaviors of SDs. The SDs have to be cast as thin films on glass slides to adapt

to CLSM observation, whereas the SD powders are made from bulk slabs to facilitate both DSC and PXRD analysis. To ensure meaningful interpretation and comparison between film-casting and milled slab samples, the preparative procedures are kept as similar as possible except for the parameters that appeal to the batch size such as the substrate of SD formation, means for solvent evaporation, and the final procedure of milling. The co-precipitation method for the preparation of Cur-PVP K30 SD differs from the melting/congealing method for Cur-PEG6000 and Cur-P407 SDs, but it does not matter because there is no need for a comparison between PVP-based and PEGs- or Poloxamers-based SDs. As PEG 6000 and P407 have a certain degree of similarity in crystallinity and melting/congealing behaviors, the preparative procedures for their SDs are kept the same. Even though the co-precipitation could also be utilized to replace melting/congealing for the preparation of both PEGs- and Poloxamers-based SDs, a conventional melting/congealing method is selected.

In conclusion, by contrasting the fluorescence of P4 with Cur autofluorescence, the existence of multiple phases in binary Cur SD systems has been revealed by CLSM. P4 could dissolve in the carrier polymer matrices in a state of solid solution, while Cur has a certain degree of solubility in the carrier matrix too. When Cur loading surpasses a critical point, crystallization happens within the SD matrix. The degree of crystallinity is positively appropriate to Cur loading. PVP K30 has the strongest ability to suppress crystallization with no Cur crystallines detected at a loading of less than 50%. For both P407 and PEG6000, crystallization starts at a Cur loading of approximately 30%. At a loading level of 20% and below, no crystallines are detected, but Cur exists as clusters of drug-rich domains. Specifically, at a loading level of 10% in the Cur-PEG6000 SD, a discrete non-crystalline phase of Cur-PEG6000 co-mix presents. Results of DSC and PXRD confirm the crystallinity of the Cur binary SD systems as revealed by the fluorescence contrasting strategy.

Declaration of competing interest

The authors declare that they have no known competing financial interests or personal relationships that could have appeared to influence the work reported in this paper.

Acknowledgment

This work was financially supported by the Science and Technology Commission of Shanghai Municipality (No. 21430760800).

Supplementary materials

Supplementary material associated with this article can be found, in the online version, at doi:10.1016/j.cclet.2023.109324.

References

[1] W.L. Chiou, S. Riegelman, J. Pharm. Sci. 60 (1971) 1281–1302.
[2] A.T. Serajuddin, J. Pharm. Sci. 88 (1999) 1058–1566.
[3] C.L. Vo, C. Park, B.J. Lee, Eur. J. Pharm. Biopharm. 85 (2013) 799–813.
[4] S.V. Bhujbal, B. Mitra, U. Jain, et al., Acta Pharm. Sin. B 8 (2021) 2505–2536.
[5] Y. Kong, W. Wang, C. Wang, et al., Int. J. Pharm. 631 (2023) 122524.
[6] K. Sekiguchi, N. Obi, Chem. Pharm. Bull. 9 (1961) 866–872.
[7] A.G. Nambiar, M. Singh, A.R. Mali, et al., AAPS PharmSciTech 23 (2022) 249.
[8] A. Butreddy, Eur. J. Pharm. Biopharm. 177 (2022) 289–307.
[9] F. Meng, U. Gala, H. Chauhan, Drug Dev. Ind. Pharm. 41 (2015) 1401–1415.
[10] L.S. Taylor, G.G.Z. Zhang, Adv. Drug Deliv. Rev. 101 (2016) 122–142.
[11] T. Van Duong, G. Van den Mooter, Expert Opin. Drug Deliv. 13 (2016) 1681–1694.
[12] K. DeBoyace, P.L.D. Wildfong, J. Pharm. Sci. 107 (2018) 57–74.
[13] F. Qian, J. Huang, M.A. Hussain, J. Pharm. Sci. 99 (2010) 2941–2947.
[14] D.N. Bikiaris, Expert Opin. Drug Deliv. 8 (2011) 1501–1519.
[15] J. Qi, Y. Lu, W. Wu, Curr. Pharm. Des. 21 (2015) 2668–2676.
[16] F. Meng, V. Dave, H. Chauhan, Eur. J. Pharm. Sci. 77 (2015) 106–111.
[17] S. Baghel, H. Cathcart, N.J. O'Reilly, J. Pharm. Sci. 105 (2016) 2527–2544.
[18] D. Gramaglia, B.R. Conway, V.L. Kett, et al., Int. J. Pharm. 301 (2005) 1–5.
[19] D. Lin, Y. Huang, Int. J. Pharm. 399 (2010) 109–115.
[20] Y. Sun, J. Tao, G.G. Zhang, et al., J. Pharm. Sci. 99 (2010) 4023–4031.
[21] B. Tian, X. Wang, Y. Zhang, et al., Pharm. Res. 32 (2015) 840–851.
[22] J.A. Baird, L.S. Taylor, Adv. Drug Deliv. Rev. 64 (2012) 396–421.
[23] Z. Chen, Z. Liu, F. Qian, Mol. Pharm. 12 (2015) 590–599.
[24] S. Baghel, H. Cathcart, N.J. O'Reilly, Eur. J. Pharm. Biopharm. 107 (2016) 16–31.
[25] S.G. Gumaste, S.S. Gupta, A.T.M. Serajuddin, AAPS J. 18 (2016) 1131–1143.
[26] R. Jog, R. Gokhale, D.J. Burgess, Int. J. Pharm. 509 (2016) 285–295.
[27] N. Li, L.S. Taylor, Mol. Pharm. 13 (2016) 1123–1136.
[28] H.S. Purohit, L.S. Taylor, Mol. Pharm. 12 (2015) 4542–4553.
[29] B. Tian, X. Tang, L.S. Taylor, Mol. Pharm. 13 (2016) 3988–4000.
[30] H.S. Purohit, J.D. Ormes, S. Saboo, et al., Pharm. Res. 34 (2017) 1364–1377.
[31] R. Yang, G.G.Z. Zhang, K. Kjoller, et al., Int. J. Pharm. 619 (2022) 121708.
[32] R. Yang, G.G.Z. Zhang, D.Y. Zemlyanov, et al., J. Pharm. Sci. 112 (2023) 304–317.
[33] L.A. Wegiel, Y. Zhao, L.J. Mauer, et al., Pharm. Dev. Technol. 19 (2014) 976–986.
[34] X. Hu, J. Zhang, Z. Yu, et al., Nanomedicine 11 (2015) 1939–1948.
[35] X. Hu, W. Fan, Z. Yu, et al., Nanoscale 8 (2016) 7024–7035.
[36] Y. Cai, X. Ji, Y. Zhang, et al., Aggregate 4 (2023) e277.
[37] H. He, C. Liu, J. Ming, et al., Aggregate 3 (2022) e163.
[38] J. Qi, X. Hu, X. Dong, et al., Adv. Drug Deliv. Rev. 143 (2019) 206–225.
[39] X. Wang, L. Qiu, X. Wang, et al., Int. J. Pharm. 573 (2020) 118840.
[40] Y. Yang, Y. Lv, C. Shen, et al., Acta Pharm. Sin. B 11 (2021) 1056–1068.
[41] Z. Huang, Y. Huang, W. Wang, et al., J. Control. Release 325 (2020) 206–222.
[42] I. Zoya, H. He, L. Wang, et al., Chin. Chem. Lett. 32 (2021) 1545–1549.
[43] Y. Jiang, Y. Jiang, Z. Ding, et al., Int. J. Nanomed. 17 (2022) 3443–3456.
[44] L. Li, S. Chunta, X. Zheng, et al., Chin. Chem. Lett. 35 (2024) 108662.
[45] B. Shen, C. Shen, W. Zhu, et al., Acta Pharm. Sin. B 11 (2021) 978–988.
[46] L. Hang, C. Shen, B. Shen, et al., Chin. Chem. Lett. 33 (2022) 4948–4951.
[47] C. Shen, Y. Yang, B. Shen, et al., Nanoscale 10 (2017) 436–450.
[48] Y. Xie, B. Shi, F. Xia, et al., J. Control. Release 270 (2018) 65–75.
[49] C.C.C. Teixeira, L.M. Mendonça, M.M. Bergamaschi, et al., AAPS PharmSciTech 17 (2016) 252–261.
[50] H. McFall, S. Sarabu, V. Shankar, et al., Int. J. Pharm. 554 (2019) 302–311.
[51] C. Muangnoi, P.R.N. Bhuket, P. Jithavech, et al., Pharmaceutics 11 (2019) 373.
[52] R. Bajracharya, S.H. Lee, J.G. Song, et al., Pharmaceutics 11 (2019) 206.
[53] X. Ji, Y. Cai, X. Dong, et al., Nanoscale 15 (2023) 9290–9296.
[54] S. Saboo, N.A. Mugheirbi, D.Y. Zemlyanov, et al., J. Control. Release 298 (2019) 68–82.
[55] S. Saboo, L.S. Taylor, Int. J. Pharm. 529 (2017) 654–666.
[56] M.J. Jackson, S.J. Toth, U.S. Kestur, et al., Mol. Pharm. 11 (2014) 3027–3038.
[57] L.I. Mosquera-Giraldo, L.S. Taylor, Mol. Pharm. 12 (2015) 496–503.
[58] S.A. Raina, D.E. Alonzo, G.G. Zhang, et al., Pharm. Res. 32 (2015) 3660–3673.
[59] M.J. Jackson, U.S. Kestur, M.A. Hussain, et al., Pharm. Res. 33 (2016) 1276–1288.
[60] L. Lindfors, S. Forssén, J. Westergren, et al., J. Colloid. Interf. Sci. 325 (2008) 404–413.